Nuclear Magnetic Resonance Structure of the Varkud Satellite Ribozyme Stem−Loop V RNA and Magnesium-Ion Binding from Chemical-Shift Mapping[†,‡]

Dean O. Campbell[§] and Pascale Legault*[,§,||]

Department of Biochemistry and Molecular Biology, University of Georgia, Athens, Georgia 30602, and Département de Biochimie, Université de Montréal, C.P. 6128, Succursale Centre-Ville, Montréal, QC, Canada H3C 3J7

Received September 21, 2004; Revised Manuscript Received November 18, 2004

ABSTRACT: An important step in the substrate recognition of the *Neurospora* Varkud Satellite (VS) ribozyme is the formation of a magnesium-dependent loop/loop interaction between the terminal loops of stem−loops I and V. We have studied the structure of stem−loop V by nuclear magnetic resonance spectroscopy and shown that it adopts a U-turn conformation, a common motif found in RNA. Structural comparisons indicate that the U-turn of stem−loop V fulfills some but not all of the structural characteristics found in canonical U-turn structures. This U-turn conformation exposes the Watson−Crick faces of the bases within stem−loop V (G697, A698, and C699) and makes them accessible for interaction with stem−loop I. Using chemical-shift mapping, we show that magnesium ions interact with the loop of the isolated stem−loop V and induce a conformational change that may be important for interaction with stem−loop I. This study expands our understanding of the role of U-turn motifs in RNA structure and function and provides insights into the mechanism of substrate recognition in the VS ribozyme.

The VS ribozyme originates from the 881-nucleotide (nt)[1] Varkud Satellite (VS) RNA, which was initially isolated from the mitochondria of certain isolates of *Neurospora* (*1*). In these mitochondria, the VS ribozyme is involved in RNA processing as part of its replication cycle (*2*). Both in vivo and in vitro, the VS ribozyme is a catalytic RNA capable of site-specific cleavage and ligation reactions (*1*, *3*−*5*). Fragments of ∼120−180 nt derived from the natural VS RNA undergo cleavage at a specific phosphodiester bond between G620 and A621 (*4*). The secondary structure of the VS ribozyme containing the minimal contiguous sequence for cleavage consists of six helical subdomains (I−VI) (Figure 1a): stem−loop I forms the substrate domain, and stem−loops II−VI comprise the catalytic domain (*6*). In vivo, the VS ribozyme likely acts in cis, since stem−loop I is found 5′ of the catalytic domain on the same RNA chain. In vitro, stem−loop I and the catalytic domain can also be synthesized as separate RNA fragments, and the catalytic domain can

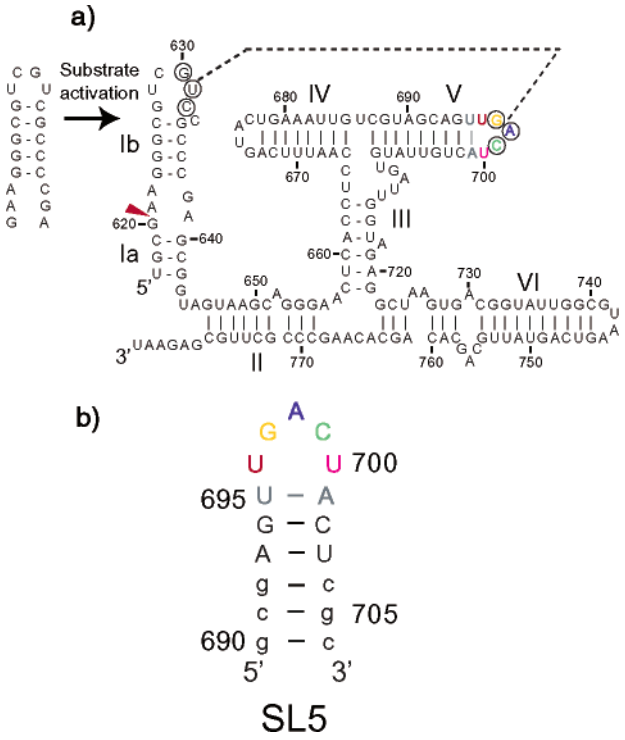

FIGURE 1: Stem−loop V RNA within the VS ribozyme. (a) Sequence and secondary structure of the *Neurospora* VS ribozyme. The cleavage site is indicated by the arrowhead. The interaction between stem−loops I and V is indicated by a dashed line, and residues involved in this interaction are circled. Upon interaction with stem−loop V, stem−loop I (subdivided into Ia and Ib) undergoes a structural change from an inactive to an active conformation. (b) Sequence and secondary structure of the stem−loop V (SL5) RNA used for NMR study. Wild-type and mutant nucleotides are represented by upper and lower cases, respectively.

[†] Supported by a National Science Foundation (NSF) Career Award (9984582) and partially from a Canadian Institutes for Health Research (CIHR) grant (117713).

[‡] Coordinates for SL5 have been deposited in the Protein Data Bank, www.rcsb.org, under Accession Number 1TBK.

* To whom correspondence should be addressed at the Département de Biochimie, Université de Montréal, C. P. 6128, Succursale Centre-Ville, Montréal, QC, Canada H3C 3J7. Phone +1 514 343-7326; fax +1 514 343-2210; e-mail pascale.legault@umontreal.ca.

[§] University of Georgia.

[||] Université de Montréal.

[1] Abbreviations: nt, nucleotide; SL5, stem−loop 5; 2D, two-dimensional; 3D, three-dimensional; HSQC, heteronuclear single quantum coherence; CT-HSQC, constant-time heteronuclear single quantum coherence; COSY, correlated spectroscopy; E.COSY, exclusive correlated spectroscopy; TOCSY, total correlation spectroscopy; MQ, multiple quantum; HETCOR, heteronuclear correlation; NOE, nuclear Overhauser effect; NOESY, nuclear Overhauser effect spectroscopy; CPMG, Carr−Purcell−Meiboom−Gill method; HMQC, heteronuclear multiple quantum correlation; TROSY, transverse relaxation optimized spectroscopy; CSA, chemical-shift anisotropy; PDB, protein data bank; RMSD, root-mean-square deviation; rRNA, ribosomal RNA.

10.1021/bi047963l CCC: $30.25
Published on Web 02/24/2005

perform cleavage in trans with multiple turnovers (*7*). The products of the VS ribozyme cleavage reaction have 5′-OH and 2′,3′-cyclic phosphate termini as found for other small catalytic RNAs, such as the hammerhead, hairpin, and HDV ribozymes (*1*).

The VS ribozyme differs from other small catalytic RNAs in its mode of substrate recognition. Most ribozymes recognize their substrate primarily via base-pairing interactions between single-stranded regions of the catalytic domain and the complementary single-stranded regions of the substrate. In the case of the *Neurospora* VS ribozyme, the catalytic domain recognizes its hairpin substrate (*7*) through tertiary interactions (*8*, *9*). The best-characterized interaction is a loop/loop interaction between stem−loops I and V, which was identified from mutagenesis and structural probing experiments (*8*). This interaction, also termed the kissing or pseudoknot interaction, involves Watson−Crick base pairing between nucleotides G630, U631, and C632 in stem−loop I and nucleotides C699, A698, and G697 in stem−loop V (see Figure 1a) (*8*). Formation of this tertiary interaction is important for efficient cleavage and ligation by the VS ribozyme (*5*, *8*).

It has been shown that the interaction of stem−loop I with stem−loop V causes a conformational change in the stem−loop I substrate (Figure 1a) (*5*, *10*). This conformational change can be triggered not only by the full catalytic domain but also by an isolated stem−loop V RNA (*5*, *10*). Upon binding to stem−loop V, stem−loop I is converted from an "unshifted" to a "shifted" conformation in which nucleotides 623−625 in helix Ib shift their base-pairing partners from nucleotides 634−636 to nucleotides 635−637, leading to a rearrangement in the cleavage site internal loop (*5*). Stem−loop I RNA mutants that cannot undergo this conformational change are not cleaved by the VS ribozyme, whereas stem−loop I mutant substrates that can adopt the shifted conformation are active in the cleavage reaction (*10*). The loop/loop interaction and the conformational change in stem−loop I are both dependent on the presence of magnesium ions (*5*, *8*, *10*).

It has been postulated from mutagenesis (*8*) and nucleotide analogue interference mapping (NAIM) (*11*, *12*) experiments that stem−loop V forms a U-turn motif, which facilitates its binding to stem−loop I. U-turns were originally identified in the anticodon and TψC loop of tRNA (*13*). They now constitute a common structural motif found in a large number of RNAs, including the hammerhead ribozyme (*14*), 23S rRNA (*15*), U2 snRNA (*16*), and HIV genomic RNA (*17*). Some of the structural characteristics of U-turns are a UNR sequence, a sharp turn in the direction of the RNA backbone after the U, formation of hydrogen bonds between U 2′-OH and R N7 and between U H3 and R 3′-phosphate, and stacking of bases after the U (*13*, *18*, *19*). The residues U696, G697, and A698 of stem−loop V constitute a UNR sequence, and mutational studies of these residues have lead to the idea that stem−loop V forms a U-turn motif (*8*). NAIM interference data indicate that substitution of the 2′-OH group of U696 by a 2′-H leads to decreased activity of the VS ribozyme, possibly due to the removal of an important hydrogen bond between U696 2′-OH and A698 N7 in the U-turn of stem−loop V (*11*, *12*). Similarly, phosphorothioate substitution of A698 3′-phosphate leads to decreased activity of the VS ribozyme, possibly due to the removal of an important hydrogen bond between one of the nonbridging oxygens of this phosphate and U696 H3, although direct divalent metal-ion binding proposed at this phosphate could also explain the loss of cleavage activity (*12*, *20*).

Like many other ribozymes, the *Neurospora* VS ribozyme provides a useful model system for studying the relationship between RNA structural motifs and their implication for RNA function (*5*, *8*, *21*). It is now well understood that functional RNAs, including ribozymes, adopt complex three-dimensional structures, which involve elaborate arrangements of double-helical subdomains (*14*, *22*). It is not always clear, however, how individual RNA motifs allow proper orientation of these various subdomains, participate in tertiary interactions, and interact with metal ions to provide the unique organization of chemical groups at the active site of ribozymes. In this paper, we present the solution NMR structure of a stem−loop V RNA in the absence of magnesium ions and show that it adopts a U-turn motif. By comparing the structural characteristics of this U-turn motif with that of canonical U-turn structures selected from the structural database, we observe that the stem−loop V RNA is missing a few important structural characteristics of canonical U-turn structures. Interestingly, the stem−loop V bases that are involved in the loop/loop interaction have their Watson−Crick faces accessible for base pairing with stem−loop I. Using chemical-shift mapping, we find that magnesium ions interact with the U-turn of stem−loop V, likely producing a conformational change in this loop. We discuss our findings in terms of the structural characteristics of U-turn motifs and in terms of substrate recognition by the VS ribozyme.

EXPERIMENTAL PROCEDURES

Sample Preparation. The 17-mer SL5 RNA was synthesized in vitro by use of T7 RNA polymerase, a double-stranded synthetic oligonucleotide template modified with C2′-methoxyl at the last two 5′-nucleotides of the coding strand (Macromolecular Resources) (*23*, *24*), and unlabeled, ^{15}N-labeled, or ^{13}C/^{15}N-labeled nucleoside triphosphates. T7 RNA polymerase and isotopically labeled nucleoside triphosphates were produced according to published procedures (*25*, *26*). SL5 was purified by denaturing 20% gel electrophoresis, dephosphorylated at its 5′-end with calf alkaline phosphatase (Roche Molecular Biochemicals), and further purified by DEAE-Sephacel chromatography (Amersham Biosciences) (*27*). The RNA sample was concentrated and the buffer was exchanged in Centricon-3 ultrafiltration devices (Millipore, MA) with NMR buffer S (10 mM Tris-d_{11}, pH 7.0, 50 mM NaCl, 0.2 mM EDTA, and 0.05 mM NaN_3) in 90% H_2O and 10% D_2O. For studies in D_2O, the RNA samples were transferred to 99.996% D_2O by multiple cycles of lyophilization and resuspension in D_2O. The concentration of the NMR samples ranged from 0.8 to 3.4 mM SL5 as determined from the absorbance at 260 nm and using a coefficient of 40 μg/mL per OD unit. Before each set of NMR experiments, the RNA sample was heated to 95 °C for 2 min and then immediately cooled in iced water.

NMR Spectroscopy. All NMR experiments were conducted at 5, 15, and 25 °C on Varian ^{Unity}Inova 600 or 800 MHz spectrometers equipped with pulse-field gradient units and actively shielded *z* gradient probes, either a ^{1}H{^{13}C/^{15}N}

Table 1: Structural Statistics

distance restraints	527
no. of NOE-derived distance restraints	498
from standard NOESY spectra	422
internucleotide	177
intranucleotide	245
from 2D ^{1}H−^{15}N CMPG-NOESY spectra	76
hydrogen-bond restraints	29
dihedral angle restraints	26
sugar pucker (δ)	13
backbone (γ)	13
total no. of restraints	553
RMSD from experimental restraints	
NOE (Å) (none > 0.1 Å)	0.0026 ± 0.0003
dihedral (deg) (none > 5°)	0.027 ± 0.015
RMSD from idealized geometry	
bonds (Å)	0.003 929 ± 0.000 018
angles (deg)	0.957 890 ± 0.000 907
impropers (deg)	0.360 240 ± 0.000 880
heavy-atom RMSDs to the minimized average structure (Å)	
overall (residues 691−705)	0.90 ± 0.14
stem (residues 691−695 and 701−705)	0.46 ± 0.07
loop (residues 696−700)	0.53 ± 0.05

triple-resonance probe or a ^{1}H{^{15}N−^{31}P} indirect detection probe. Assignments of ^{1}H, ^{13}C, ^{15}N, and ^{31}P nuclei in SL5 were obtained from two-dimensional (2D) and three-dimensional (3D) homonuclear and heteronuclear NMR experiments. All nonexchangeable protons and their attached carbons were assigned from the following experiments collected at 25 °C in D_2O: 2D ^{1}H−^{13}C CT-HSQC (*28*, *29*); 2D ^{1}H−^{15}N MQ-(HC)N(C)H (*30*); 3D HCCH-COSY (*31*); 3D HCCH-TOCSY (*31*); and a 3D ^{13}C-edited HMQC-NOESY (*32*). The exchangeable protons and their attached nitrogens were assigned from the following experiments collected at 25 °C in H_2O: imino- and amino-optimized 2D ^{1}H−^{15}N HSQC (*33*); 2D H(NCCC)H for uracil and cytosine residues (*34*); 2D H(NC)-TOCSY-(C)H for guanosine residues (*35*); 2D (H)N(C)-TOCSY-(C)H for adenosine residues (*36*); 2D ^{1}H−^{15}N CPMG-NOESY (*37*); and a 2D ^{1}H−^{1}H flip-back watergate NOESY (*38*, *39*). A 2D ^{1}H−^{15}N HMQC optimized for transfers via $J = 7.0$ Hz (*40*) was collected at 25 °C in D_2O for assignment of uridine N3 nitrogens. A 2D ^{1}H−^{31}P HETCOR (*41*) spectrum was also collected in D_2O at 25 °C for the assignment of the ^{31}P resonances. Distance restraints were obtained from a 2D ^{1}H−^{1}H flip-back watergate NOESY spectrum collected in H_2O at 25 °C with a mixing time of 400 ms (*38*, *39*), 2D ^{1}H−^{15}N CPMG-NOESY spectra collected at 5 and 25 °C in H_2O with mixing times of 150 ms (*37*), and 3D ^{13}C-edited HMQC-NOESY spectra (*32*) collected in D_2O at 25 °C with mixing times of 90 ms and 180 ms. The hydrogen-bond restraints were determined from 2D HNN-COSY spectra collected at 25 °C (*42*, *43*). Restraints for the δ torsion angle were obtained from experiments collected at 25 °C in D_2O: 2D DQF-COSY, 3D HCCH E.COSY (*44*), and 2D ^{1}H−^{13}C CT-TROSY for measurement of CSA-dipolar cross-correlated rate constants (at 600 and 800 MHz) (*45*). All spectra were processed with the NMRPipe/NMRDraw package (*46*) and analyzed with NMRView (*47*). ^{1}H, ^{13}C, and ^{15}N chemical shifts were referenced at 25 °C to an external standard of 2,2-dimethyl-2-silapentane-5-sulfonic acid (DSS) at 0.00 ppm (*48*), and ^{31}P chemical shifts were referenced at 25 °C to an external standard of 85% phosphoric acid at 0.00 ppm.

Structure Calculation. The distance restraints from the 2D ^{1}H−^{1}H NOESY and 3D ^{13}C-edited HMQC-NOESY spectra were separated into four ranges: strong (1.8−3.0 Å), medium (1.8−4.1 Å), and weak (1.8−5.5 Å), based on the intensities of peaks observed at a mixing time of 90 ms, and very weak (1.8−7.0 Å), for signals observed only at mixing times greater than 90 ms. The distance restraints obtained from the 2D ^{1}H−^{15}N CPMG-NOESY were given ranges of either 1.8−5.5 or 1.8−7.0 Å on the basis of cross-peak intensities. The distance restraints were calibrated on the basis of the cross-peaks intensities and by comparison with NOE cross-peaks involving protons separated by known intraresidue distances. Two-dimensional HNN-COSY spectra were collected to detect $^2J_{NN}$ couplings across hydrogen bonds in Watson−Crick base pairs (*42*, *43*). Because of the strong NMR evidence (NOESY and HNN-COSY) for the formation of the A-U and G-C Watson−Crick base pairs in the stem of SL5, canonical distance restraints were employed to define the hydrogen-bonding pattern and planarity of the first five base pairs in the stem of SL5 (residues 690−694 and 702−706). We obtained limited NOE data for the U695-A701 base pair; therefore, in this case, only the U695 N3 to A701 N1 distance was defined (2.82 ± 0.1 Å) on the basis of the HNN-COSY data. Sugar pucker conformations were derived from 2D DQF-COSY, 3D HCCH E.COSY (*44*), and 2D ^{1}H−^{13}C CT-TROSY experiments (*45*). All the sugar puckers except for the loop residues 697−700 were set to C3′-endo (δ = 86° ± 10°). The γ torsion angle restraints were derived from comparative analyses of NOE data (*49*). The γ angles for all the residues except the loop residues 697−700 were set to the gauche$^+$ conformation (γ = 60° ± 20°).

Three-dimensional structures were calculated with restrained molecular dynamics and simulated annealing in X-PLOR−NIH 2.0.6 (*50*, *51*) by a modified version of a previously reported protocol (*52*). The experimental restraints described in Table 1 were used along with restraints to maintain the covalent structure and stereochemistry of the RNA. The CHARMM force field was used with the ribose bond angles modified to prevent flattening of the ring. The same reduced force field was used at all steps except for the first energy minimization. This force field consists of bond, angle, improper (stereochemical), and repulsive van der Waals energy terms and NOE and torsion angle pseudoenergy terms. Electrostatic contributions were not included in

the force field. Initial structures were generated by randomizing the backbone (α, *β*, *γ*, *δ*, *ϵ*, and *ζ*) and *χ* angles followed by an energy minimization with a force field that included bond, angle, improper, and repulsive van der Waals energy terms. A first cycle (29 ps) of high-temperature dynamics (3000 K) was used to introduce the NOE and torsion angle pseudoenergy terms, gradually increasing the weight on the van der Waals energy term and gradually transforming the X-PLOR pseudoenergy NOE term from a soft to a square well. The system was then slowly cooled (3000 to 300 K in 6.25 ps) and energy-minimized. A second cycle (10 ps) of high-temperature dynamics (3000 K) was then used in which the weight on the torsion angle pseudoenergy term was reduced, slowly increased, reduced again, and then slowly increased up to its final value. The system was subsequently cooled very slowly (3000 to 300 K in 12.5 ps) and energy-minimized. This second cycle helps to improve the percentage of accepted structures. Starting from a set of 100 structures with randomized torsion angles, 61 structures satisfied the experimental restraints (no distance violation > 0.1 Å and no torsion angle violation > 5°). From these 61 structures, the 10 lowest-energy structures were selected for further analysis and used to calculate an average structure that was minimized against experimental restraints. All structures were visualized with MOLMOL (*53*) and analyzed with MOLMOL and CURVES (*54*).

Metal-Ion Binding Studies. Two 1.0 mM samples of $^{13}C/^{15}N$-labeled SL5 in NMR buffer A (10 mM Tris-d_{11}, pH 7.0, 0.05 mM NaN_3, and 50 mM NaCl) and in 100% D_2O were titrated with metal salts, one with 99.995% $MgCl_2$ (Sigma−Aldrich) and the other one with NaCl. The titrations were both carried out by adding an increasing amount of a concentrated salt solution directly to the NMR sample. For the $MgCl_2$ titration, the magnesium ion concentrations were 0, 0.25, 0.50, 0.75, 1.0, 2.0, 3.0, 5.0, 10, 20, 30, 40, 50, and 130 mM. For the NaCl titration, the sodium ion concentrations were 50, 100, 150, 250, 350, and 500 mM. Chemical-shift changes were monitored at each salt concentration by collecting 2D $^1H-^{13}C$ CT-HSQC spectra (*29*). To remove the ambiguity in chemical shift assignments at high salt concentrations, complete ^1H and ^{13}C assignments were redone for SL5 at 40 mM $MgCl_2$ (D. Campbell and P. Legault, unpublished data). To quantify the chemical-shift changes [Δ_T in parts per million (ppm) ± 0.05 ppm], the following equation was used: $\Delta_T = [(\Delta_H)^2 + (R\Delta_C)^2]^{1/2}$, where Δ_H is the ^1H chemical-shift change, Δ_C is the ^{13}C chemical-shift change, and R is a scaling factor calculated as the ratio between the ^1H and ^{13}C chemical-shift ranges for a particular type of $^1H/^{13}C$ pair (*55*). The change in chemical shift as a function of $MgCl_2$ concentration was plotted for all the $^1H/^{13}C$ pairs that had a Δ_T value > 0.3 ppm at the end of the titration. These binding data were used to calculate apparent K_ds for magnesium-ion binding. Assuming fast exchange and a 1:1 stoichiometry, the apparent K_ds were calculated by fitting the following equation: $\Delta_{obs} = (\Delta_T)/(2[RNA]_T)\{([Mg]_T + [RNA]_T + K_d) - (([Mg]_T + [RNA]_T + K_d)^2 - (4[Mg]_T[RNA]_T))^{1/2}\}$, where Δ_{obs} is the observed ^1H or ^{13}C chemical-shift change at each $MgCl_2$ concentration, Δ_T is the total change in ^1H or ^{13}C chemical shift, and $[Mg]_T$ and $[RNA]_T$ are the total concentrations of magnesium ion and RNA, respectively (*56*, *57*). Apparent K_ds were calculated from resolved $^1H-^{13}C$ CT-HSQC signals that belong to loop residues based on the changes in both ^1H and ^{13}C chemical shifts; two apparent K_d values were therefore obtained for each HSQC signal. All binding curves were fitted by the least-squares analysis function of GRACE (http://plasma-gate.weizmann.ac.il/Grace/).

Relaxation Measurements. The ^{13}C $T_{1\rho}$ measurements on the aromatic C6/C8 carbons were performed on $^{13}C/^{15}N$-labeled SL5 in 10 mM Tris-d_{11}, pH 7.0, 50 mM NaCl, 0.2 mM EDTA, 0.05 mM NaN_3, and 100% D_2O. Measurements were performed at 600 MHz and 25 °C with the pulse sequence from Yamazaki et al. (*58*). Nine different spin-lock delays T were used: 4, 8, 12, 16, 24, 32, 40, 48, and 60 ms. For $T < 20$ ms, 20 ms $\leq T <$ 40 ms, 40 ms $\leq T <$ 60 ms, and $T = 60$ ms, $k = 0$, 1, 2, and 3 ^1H 180° pulses, respectively, were applied during the ^{13}C spin-lock interval according to the scheme $[T/(2k) - {}^1H\ 180° - T/(2k)]_{k,k\neq 0}$ in order to prevent cross-correlation effects that can lead to overestimation of ^{13}C $T_{1\rho}$ values (*59*). The ^{13}C carrier was positioned in the center of the C6/C8 region (139.7 ppm), and a spin-lock power of 3.8 kHz was used. At the largest offset for C6 and C8 resonances, which range from 135.8 to 143.6 ppm, the tip angle of the spin-lock axis was 81°. Relaxation times were extracted by nonlinear curve fitting of the maximum signal intensity from the 2D spectra by use of GRACE (http://plasma-gate.weizmann.ac.il/Grace/). A two-parameter fit $\{I(t) = [A_0e(-t/T_{1\rho})]\}$ of the experimental decay curve gave low correlation coefficients, likely because of poor signal-to-noise at the longer spin-lock delays. A three-parameter fit $\{I(t) = [A_0e(-t/T_{1\rho})] + A_2\}$ was therefore employed (*60*), and in all cases the correlation coefficients of the fit were ≥0.99. Reported error bars are taken from the uncertainties in the nonlinear fit.

RESULTS

Conformation of SL5. To gain insights into substrate recognition by the VS ribozyme, we synthesized a 17-nucleotide RNA fragment of stem−loop V, termed SL5 (Figure 1b), for NMR structural determination. Based on the secondary structure of the VS ribozyme (*6*), SL5 was designed to form a hairpin structure that retains the natural sequence within its five-member terminal loop and its three closing base pairs (Figure 1b). The first three base pairs of the stem were mutated to increase yields of in vitro transcription by T7 RNA polymerase (*23*). It has been previously determined that the identity of the nucleotides in the stem of helical domain V is not important for catalytic activity as long as base pairing is maintained (*6*). In addition, chemical modification experiments indicate that SL5 (Figure 1b) is capable of shifting the conformation of an isolated stem−loop I to its active conformation in the presence of Mg^{2+} (A. Andersen, R. Collins, and P. Legault, unpublished results) (*10*). To clearly understand the effect of Mg^{2+} on complex formation, we decided to first determine the structure of SL5 in the absence of Mg^{2+} and then investigate the effect of Mg^{2+} on the SL5 structure, which may or may not require complete structure determination in the presence of Mg^{2+}. The buffer conditions (10 mM Tris-d_{11}, pH 7.0, 50 mM NaCl, and 0.05 mM NaN_3) chosen for structure determination are therefore compatible with catalysis, but only after Mg^{2+} is added (*1*).

To ensure that SL5 forms a hairpin and not a duplex under NMR conditions, SL5 was first analyzed by equilibrium

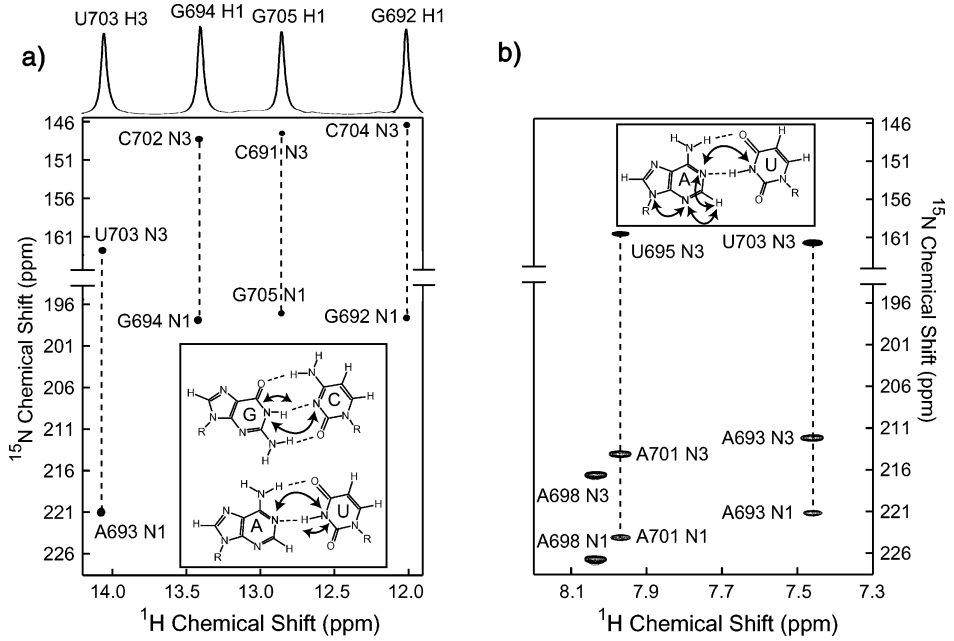

FIGURE 2: Watson−Crick base pairs in SL5. (a) Two-dimensional spectrum of an HNN-COSY experiment used to detect $^{2}J_{NN}$ couplings across hydrogen bonds in Watson−Crick base pairs. The $^{2}J_{NN}$ coupling between the N1 of the purines and the N3 of the pyrimidines of paired residues was detected via the intervening imino proton (inset). The 1D imino proton spectrum is shown above the 2D HNN-COSY spectrum. (b) Two-dimensional spectrum of a modified 2D HNN-COSY experiment used to detect $^{2}J_{NN}$ couplings across hydrogen bonds in Watson−Crick A−U base pairs. The $^{2}J_{NN}$ coupling between the N1 of the adenine and the N3 of the paired uridine was detected via the nonexchangeable adenine H2 (inset). The spectra in panels a and b were collected at 25 °C on a 600 MHz NMR spectrometer, with SL5 samples containing (a) 90% D_2O/10% H_2O and (b) 100% D_2O.

ultracentrifugation. Ultracentrifugation studies indicated that this RNA forms a homogeneous sample of unimolecular mass (~6 kDa; data not shown) at low concentration (2 μM). Native gel electrophoresis indicates that this conformation is stable at RNA concentrations of 2 μM−2 mM (not shown). The SL5 RNA also gave high-quality NMR data at high concentrations (0.8−3.5 mM), consistent with a single conformation, and small aromatic proton line widths (2.5−5 Hz) were indicative of hairpin formation. In addition, formation of a duplex would likely result in stabilization of a U-U base pair; however, no evidence of such a base pair has been obtained from the NMR data. Additional broader signals were present in the NMR spectra when we omitted to heat and immediately cool the sample prior to collecting the NMR data. It was concluded that the hairpin conformation of SL5 slowly interconverts to a duplex form over a period of weeks. We therefore took the necessary precaution to collect the NMR data on the hairpin conformation exclusively.

SL5 Structure Determination. The NMR structure of SL5 was obtained by standard homonuclear and heteronuclear NMR methods with unlabeled, ^{15}N-labeled, and ^{13}C/^{15}N-labeled RNAs, as described under Experimental Procedures. Assignment of ^{1}H, ^{13}C, ^{15}N, and ^{31}P nuclei in SL5 were obtained by standard methods and are summarized in Table S1 (Supporting Information).

The combination of the NOESY and HNN-COSY experiments (*42*, *43*) gave direct evidence for base pairing in the stem of SL5. We observed only four imino proton signals in the 1D ^{1}H spectrum of SL5 (Figure 2a). We did not observed the G690 imino proton at 25 °C; this is typically the case for the first G-C base pair of RNA stems due to fraying of the base pair. On the basis of NOE connectivities, the observed imino proton signals were easily assigned to guanine and uridine bases of the four internal base pairs in the stem, C691-G705, G692-C704, A693-U703, and G694-C702. In addition, we obtained unambiguous evidence for the formation of these base pairs from a 2D HNN-COSY spectrum collected to detect $^{2}J_{NN}$ couplings across hydrogen bonds in Watson−Crick base pairs (Figure 2a) (*42*). This experiment provides correlations between the guanine or uridine imino proton (G H1 or U H3), its bonded imino nitrogen, and the imino nitrogen of the paired residue (C N3 or A N1). We obtained these correlations for the C691-G705, G692-C704, G694-C702, and A693-U703 base pairs (Figure 2a). One limitation of this HNN-COSY experiment is that $^{2}J_{NN}$ couplings across hydrogen bonds can only be detected if the intervening imino proton is observable. Therefore, it did not provide evidence for the U695-A701 base pair predicted from the secondary structure model (Figure 1) (*6*). To verify the presence of this base pair, we used a modified version of the HNN-COSY experiment that allows detection of $^{2}J_{NN}$ couplings across hydrogen bonds in A-U base pairs via the nonexchangeable adenine H2 (Figure 2b) (*43*). For all adenine residues, this experiment provides intrabase correlations between the adenine H2 and the adenine N1, N3, and N9 (not shown). For adenines in Watson−Crick A-U base pairs, this experiment also provides a correlation between the adenine H2 and the N3 of the paired uridine. As expected, an A H2 to U N3 correlation was not observed for A698 in the loop but was observed for the well-defined A693-U703 base pair (Figure 2b). We also observed a correlation between A701 H2 and a uridine N3 signal (Figure 2b). This N3 chemical shift was unambiguously assigned to U695 N3 on the basis of a U695 N3−U695 H5 correlation observed in a long-range ^{1}H−^{15}N HMQC (not shown) (*40*). The modified HNN-COSY spectrum helped confirm the presence of a Watson−Crick U-A

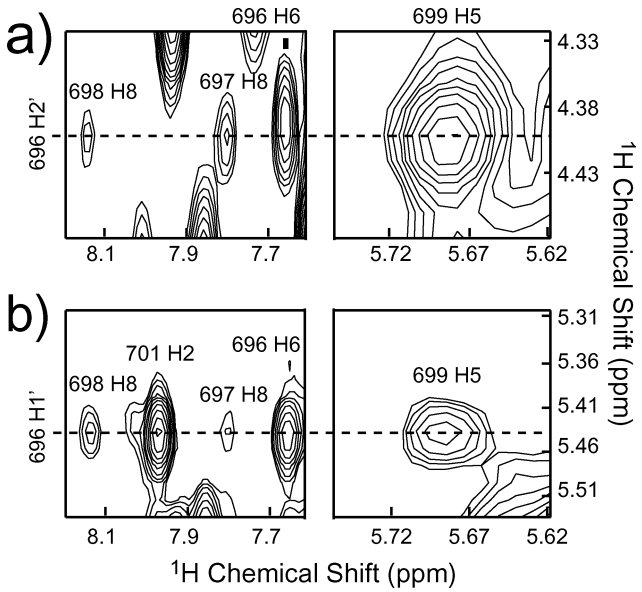

FIGURE 3: Regions from 3D ^{13}C-edited HMQC-NOESY spectra showing characteristic NOEs of the SL5 loop. (a) Region of the spectrum collected with a 90 ms mixing time and taken at the ^{13}C frequency of U696 C2′ (75.3 ppm). (b) Region of the spectrum collected with a 180 ms mixing time and taken at the ^{13}C frequency of U696 C1′ (93.6 ppm). The spectra in panels a and b were collected in 100% D_2O at 25 °C on a 600 MHz NMR spectrometer.

base pair between U695 and A701 in the absence of a detectable imino proton for U695.

In addition to confirming base pairing in the stem, the NMR data indicate that the residues in the stem (G690−U695 and A701−C706) form a typical A-form helix. Intra- and interresidue NOE patterns are characteristic of A-form helical geometry (*49*). We analyzed three NMR experiments to determine sugar pucker conformation: 2D DQF-COSY for measurement of $^3J_{H1'-H2'}$ coupling constants, 3D HCCH E.COSY for measurement of $^3J_{H1'-H2'}$ and $^3J_{H3'-H4'}$ coupling constants (*44*), and 2D ^{1}H−^{13}C CT-TROSY for measurement of CSA-dipolar cross-correlated rate constants (*45*). All three experiments indicated that residues in the stem (G690−U695 and A701−C706) as well as residue U696 adopt a C3′-endo sugar pucker conformation. Comparative analyses of NOE data, also indicated that all residues in the stem (G690−U695 and A701−C706) as well as residue U696 have their γ torsion angles in the gauche$^+$ conformation (*61*). The combination of torsion angle and NOE data (not shown) indicated that the A-form helix topology extends to U696 on the 5′-strand of the RNA. For residues G697−U700, the available NMR data indicated that theirs sugars exist as a mixture of rapidly interconverting C3′-endo and C2′-endo conformers (not shown). Therefore, γ and δ torsion angles of only residues G690−U696 and A701−C706 were constrained for structure calculation.

NOEs that are not characteristic of A-form geometry were observed in the loop of SL5 and represent important features of this loop, including the stacking pattern and the position of phosphate backbone reversal (Figures 3 and 4). We observed NOEs between H2′ of U696 and the protons A698 H8, G697 H8, U696 H6, and C699 H5 (Figure 3a) and between H1′ of U696 and the protons A698 H8, A701 H2, G697 H8, U696 H6, and C699 H5 (Figure 3b). These NOEs from U696 to residues G697, A698, C699, and A701 indicate that there is a sharp turn in the loop after U696, which places

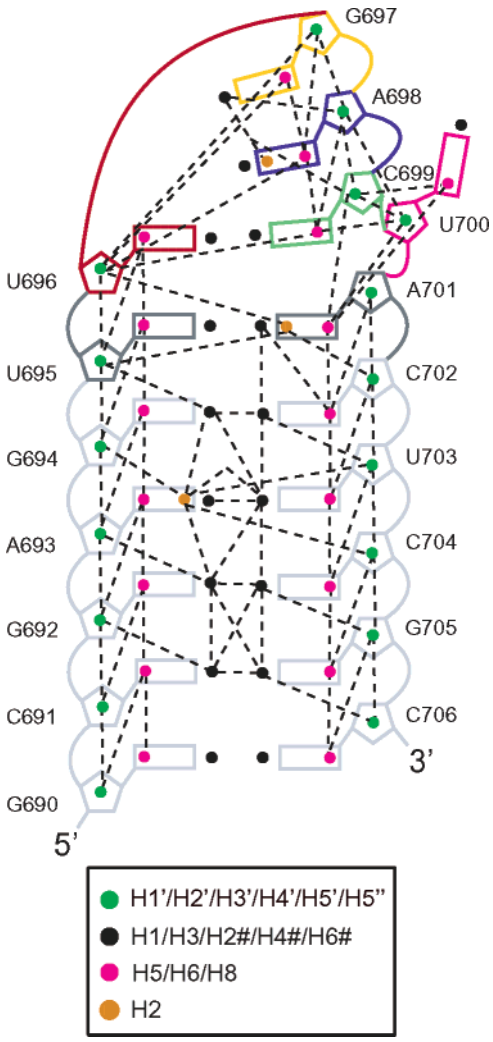

FIGURE 4: Summary diagram of the interresidue NOEs used in the structure calculation of SL5. Dashed lines represent one or more interresidue NOE(s) observed between two protons as defined in the legend.

U696 in a central location with respect to these following loop residues. Additional evidence for this turn is the absence of base-to-base NOEs between U696 and G697 (Figure 4), suggesting that these bases are not stacked on each other. The sequential ribose-to-base and base-to-base NOEs continue from G697 through to C699, similarly to what is observed for the base-paired stem. These data suggest that G697 stacks on A698 and that A698 stacks on C699, but at U700 there is a disruption of this pattern. Nonsequential NOEs between the ribose of C699 and the base of A701 combined with the absence of base-to-base NOEs between C699 and U700 suggests that the base of U700 is somewhat extruded from the loop (Figure 4). In addition, an NOE between the H4′ of A698 and the H1′ of U700 provides evidence that the ribose of U700 also adopts an unusual position within this loop.

A schematic of the observed NOEs summarizes the distance information used for structure calculation and provides an initial representation of the SL5 structure (Figure 4). In addition to NOE-derived distance restraints, we used hydrogen-bonding restraints from the HNN-COSY experiments and torsion angle restraints (see Experimental Procedures) as input for structure calculation. Three-dimensional structures were calculated by use of restrained molecular

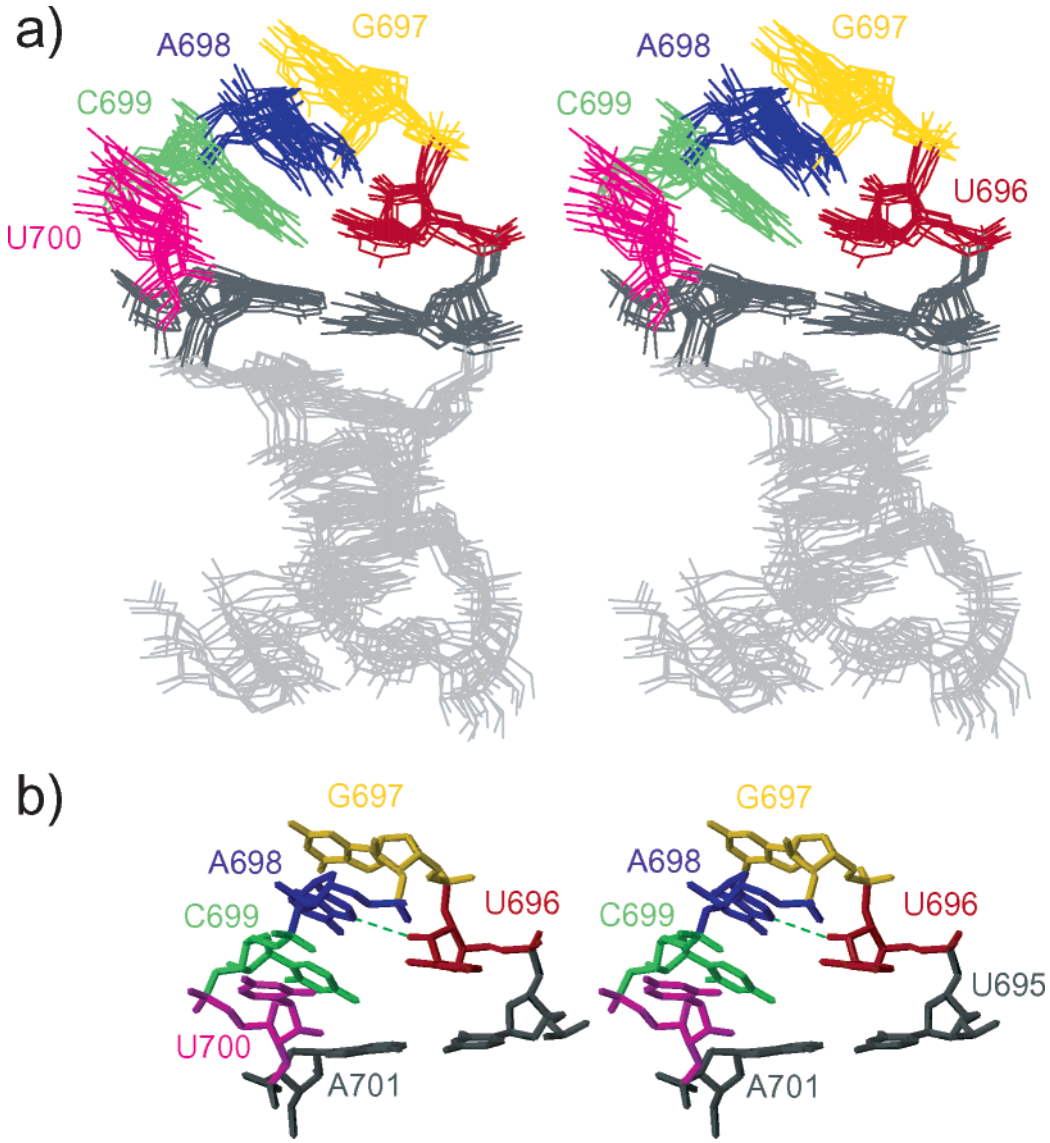

FIGURE 5: The loop of SL5 forms a U-turn motif. (a) Stereoview of the superposition of the 10 lowest-energy structures of SL5 on the minimized average structure. The superposition was obtained by minimization of pairwise heavy-atom RMSD of each lowest-energy structure to the minimized average structure (residues 691−705). (b) Stereoview of the minimized average structure of the SL5 loop showing some characteristics of U-turn motifs: the sharp turn in the backbone between U696 and G697; the short distance (2.8 Å) between the U696 2′-OH and A698 N7 (dashed line); and the stacking of the three bases following the turn. For simplicity, only heavy atoms are shown in panels a and b.

dynamics and simulated annealing. The 10 lowest-energy structures that satisfied our experimental restraints (no distance violation >0.1 Å and no torsion angle violation >5°) were retained for analysis. An average structure was calculated from these low-energy structures and was further minimized against experimental restraints. The structural statistics (Table 1) indicate that the structure of SL5, including its terminal loop, is well defined by the NMR data. The RMSD from the minimized average structure is 0.90 ± 0.14 Å for the SL5 RNA (residues 691−705) and 0.53 ± 0.05 Å for the SL5 loop (residues 696−700). The superposition of the 10 lowest-energy structures on the minimized average structure (Figure 5a) also illustrates that the overall precision of the SL5 structure is very good.

SL5 Loop Forms a Loose U-Turn Motif. As predicted from the secondary structure model (*6*), SL5 forms a hairpin characterized by a six-base-pair stem and a five-membered terminal loop (Figure 5). The SL5 stem adopts a typical A-form helix. The U695 imino proton was not observed in our NMR data, and only a few distance restraints were used to constrain the U695-A701 base pair in the structure calculation. However, we find that this base pair adopts a canonical Watson−Crick U-A base pair that is stacked on the G694-C702 base pair and is part of the A-form helix. On the 3′-strand, base stacking is continuous within the base-paired stem only (A701−C706), whereas on the 5′-strand base stacking extends beyond the stem residues (G690−U695) through U696, the first member of the loop. U696 is, however, not involved in any base-pairing interactions with U700 or other loop residues. Immediately after U696, there is a sharp turn in the direction of the backbone of SL5 (Figure 5). The next three bases after the turn (G697−C699) are all stacked on each other and their Watson−Crick faces are exposed to the solvent. The final residue in the loop, U700, has its base completely extruded from the bases of the other residues in the loop and in the stem. As can be seen from the superposition in Figure 5a, the orientation of the U700 base is not as well defined as that of other bases in the loop.

Table 2: Characteristics of Canonical U-Turn Structures and Their Occurrence in SL5

U-turn characteristics	occurrence in SL5
UNR sequence	yes (U696, G697, A698)
noncanonical flanking base pair	no (Flanking base pair is the Watson−Crick U695-A701 base pair)
sharp turn in backbone	yes (α angle in 10 lowest-energy structures: $116° \pm 7°$)
stacking of bases immediately after turn	yes (stacking of G697, A698, and C699)
stacking of U base and R 5′-phosphate group	no
H-bond between U 2′-OH and R N7	yes (U696 O2−A698 N7 distance range in 10 lowest-energy structures: 2.91−3.93 Å)
H-bond between U H3 and R 3′-phosphate group	no (U696 N3−A698 3′-P distance range in 10 lowest-energy structures: 8.19−9.18 Å)

Table 3: Hydrogen-Bond Distances in the U-Turn of SL5 and in Selected Canonical U-Turn Structures from the PDB

RNA	PDB entry	U O2′−R N7 (Å)	U N3−R 3′-P (Å)
SL5[a]	1TBK	3.43	8.65
loop 690 of eukaryotic 16S-like rRNA[b] (*66*)	1FHK	2.75	4.42
HIV-1 A-rich loop[b] (*17*)	1BVJ	2.86	4.21
U2 snRNA[a] (*16*)	2U2A	3.04	4.19
hammerhead ribozyme[c] (*73*)	300D	3.07	4.39
TψC anticodon loop of tRNA^{Phe} (yeast)[c] (*74*)	1EHZ	2.37	4.17

[a] Mimimized average structure. [b] Best representative conformer in the ensemble of NMR structures. [c] X-ray structure.

However, in all 10 final structures and in the minimized average structure (Figure 5b), the U700 base bulges out of the loop and stacks on the 5′-phosphate group of C699. With the exclusion of the U700 base from the interior of the loop, it seemed possible for the C699 base to stack on the A701 base and form a base-pairing interaction with U696. However, this is not the case in any of the 10 lowest-energy structures. Instead, the C699 base is angled toward the base of A701, and C699 is too far from U696 to form any base-pairing interaction with this residue.

The overall geometry of the SL5 loop resembles that of a U-turn motif. The characteristics of a canonical U-turn structure are a UNR sequence (U = uracil, N = any base, and R = purine), a non-Watson−Crick base pair involving the nucleotide 5′ of the UNR sequence, a sharp turn in the backbone after the U, stacking of the bases 3′ of the U, stacking of the U base with the 5′-phosphate group of the R, and two hydrogen bonds involving the U residue (*13*, *18*, *19*). These hydrogen bonds are between the U 2′-OH and the R N7 and between the U H3 and the 3′-phosphate group of the R. The U-turn characteristics of SL5 are summarized in Table 2. In SL5, the UNR sequence is represented by U696, G697, and A698. As opposed to canonical U-turn structures, the nucleotide U695 5′ of the UNR sequence forms a Watson−Crick U-A base pair with A701. We observed a sharp turn in the backbone after U696, which is characterized by an unusual value of the α torsion angle of G697 ($116° \pm 7°$ in the 10 lowest-energy structures). The three bases immediately after the turn (G697, A698, and C699) are stacked on each other. However, the base of U696 does not stack with the 5′-phosphate group of A698. As for the two hydrogen bonds that are known to stabilize the U-turn motif, only one is present in SL5. The distance between U696 2′-OH and A698 N7 is 2.77 Å in the minimized average structure, which is indicative of a hydrogen bond. However, U696 H3 and the 5′-phosphate group of C699 are 8.65 Å apart in the minimized average structure and are clearly not close enough to form a hydrogen bond with each other. We have compared the heavy-atom distances that are characteristic of U-turn motifs in SL5 with those of a few selected canonical U-turns in other RNA structures (Table 3). The U O2′ to R N7 distance of SL5 is close to the range observed for canonical U-turn structures, whereas the U N3 to R 3′-P distance is much longer than the range observed for canonical U-turn structures. In summary, SL5 forms a U-turn motif but lacks some of the structural characteristics found in canonical U-turn structures. We are referring to the U-turn of SL5 as a loose U-turn motif to emphasize the contrast between its structure and that of the more compact backbone fold adopted by canonical U-turn structures.

Effect of Metal Ions on the SL5 RNA Structure. The catalytic activity of the VS ribozyme requires the presence of metal ions. Certain divalent and monovalent salts support catalysis to various degrees, with magnesium being the most likely catalytically active biological cation (*62*, *63*). It has been shown that magnesium ions are necessary for formation of the loop/loop interaction between stem−loops I and V (*8*, *10*). In stem−loop V, the 5′-phosphate of C699 has been implicated in direct divalent metal-ion coordination from manganese rescue of phosphorothioate inhibition (*20*). We therefore used chemical-shift mapping to investigate the effect of $MgCl_2$ on the structure of SL5 and to possibly identify Mg^{2+}-binding site(s). A $MgCl_2$ titration was performed under the same conditions used for structure determination by several additions of concentrated $MgCl_2$ to achieve final $MgCl_2$ concentrations ranging from 0 to 130 mM. After each $MgCl_2$ addition, a 2D $^1H-^{13}C$ CT-HSQC (*28*, *29*) spectrum was collected to monitor chemical-shift changes. Almost all the peaks observed in the $^1H-^{13}C$ CT-HSQC spectrum were affected by addition of $MgCl_2$ as illustrated for the H6−C6/H8−C8 region (Figure 6a). Changes in ^1H and ^{13}C chemical shifts attain their midpoint around 2−3 mM $MgCl_2$, and in most cases only small changes are observed between 30 and 130 mM. Native gel electrophoresis experiments of SL5 at 40 mM $MgCl_2$ indicate that SL5 remains in a hairpin conformation at high $MgCl_2$ concentrations (not shown); therefore the observed chemical-shift changes do not result from duplex formation. Total changes in ^1H and ^{13}C chemical shifts (Δ_T) between 0 and 130 mM $MgCl_2$ were calculated for all the well-resolved peaks in the $^1H-^{13}C$ CT-HSQC spectrum (Figure 6b).

To ascertain that the chemical-shift changes were not simply a result of increased ionic strength (*I*), we compared the total changes in chemical shifts obtained at 130 mM

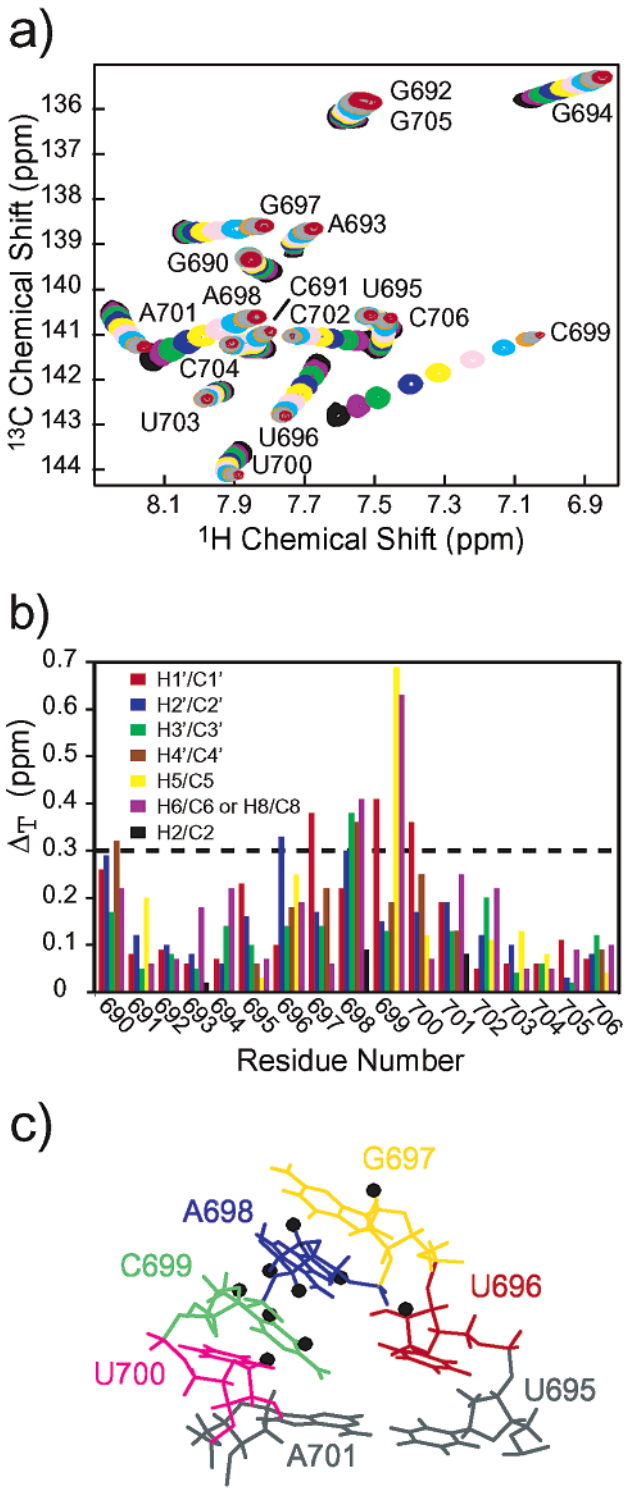

FIGURE 6: Effect of magnesium ions on SL5 RNA. (a) Overlay of the H6−C6/H8−C8 region of 2D ^{1}H−^{13}C CT-HSQC spectra of SL5 at selected points of the $MgCl_2$ titration. Spectra are shown for 0 mM (black), 0.5 mM (purple), 1.0 mM (green), 2.0 mM (blue), 3.0 mM (yellow), 5.0 mM (pale violet), 10 mM (pale blue), 30 mM (orange), 50 mM (gray), and 130 mM (red) $MgCl_2$. Peak labels are adjacent to the last point of the $MgCl_2$ titration. These spectra were collected in 100% D_2O at 25 °C on a 600 MHz NMR spectrometer. (b) Chemical-shift changes (Δ_T values) after addition of 130 mM $MgCl_2$ for the resolved peaks from the ^{1}H−^{13}C CT-HSQC spectra. (c) Summary of the magnesium-ion binding data on the minimized average structure of the SL5 loop. Significant chemical-shift changes after addition of 130 mM $MgCl_2$ ($\Delta_T > 0.3$ ppm) were indicated by a black sphere on the corresponding hydrogen atom (U696 H2′; G697 H1′; A698 H2′, H3′, H4′, and H8; C699 H1′, H5, and H6; and U700 H1′).

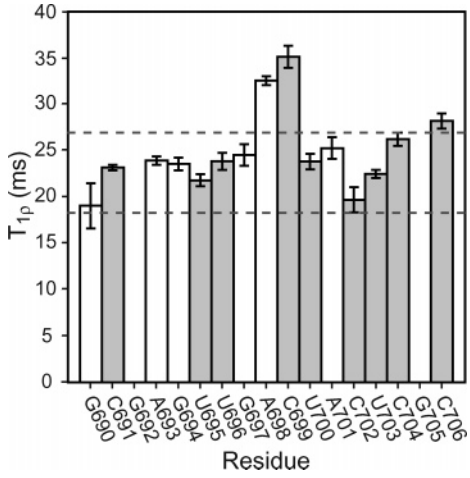

FIGURE 7: Histogram of $T_{1\rho}$ values for purine C8 and pyrimidine C6 base resonances in SL5 RNA. The values for G692 and G705 are not reported because of spectral overlap, which prevented accurate analysis. Open bars and shaded bars indicate purine and pyrimidine residues, respectively. The horizontal dashed lines indicate the range of values observed in helical regions, excluding the terminal base pairs.

$MgCl_2$ in NMR buffer that contained 50 mM NaCl ($I = 0.44$ M) with those obtained in NMR buffer supplemented with 450 mM NaCl ($I = 0.50$ M). Although chemical-shift changes were observed in the presence of 500 mM NaCl (Figure S1, Supporting Information), the magnitude of these changes was usually smaller, particularly for loop residues, than what we observed with 130 mM $MgCl_2$ in the presence of 50 mM NaCl (Figure 6b). These results indicate that the observed chemical-shift changes may be partially due to ionic strength effects but that specific magnesium-ion binding must be inferred to explain the larger chemical-shift changes observed with magnesium ions.

The largest Mg^{2+}-dependent chemical-shift changes ($\Delta_T > 0.3$ ppm) were observed for SL5 loop residues, and these changes were mapped on the structure of SL5 (Figure 6c). All residues in the loop are affected by $MgCl_2$; therefore it is not possible to precisely map one or more Mg^{2+}-binding sites by use of these chemical-shift changes. Furthermore, the chemical-shift changes in the loop not only may be due to the presence of one or more local charges but also may result from conformational changes in the SL5 loop. Apparent K_ds for magnesium ions were calculated on the basis of Mg^{2+}-dependent ^{1}H and ^{13}C chemical-shift changes for the 34 resolved signals of the SL5 loop residues (U696−U700). We obtained an average apparent K_d ($\pm\sigma$) of 2.4 ± 0.5 mM for magnesium-ion binding to the SL5 loop.

Evidence of Internal Motion in the SL5 Loop from ^{13}C Relaxation. Measurement of ^{13}C $T_{1\rho}$ relaxation times has proven useful to probe conformational dynamics in RNA (*64*). It allows for identification of dynamics on the picosecond to nanosecond time scale when $T_{1\rho}$ values are larger than those of rigid residues and for identification of dynamics on the microsecond to millisecond time scale when $T_{1\rho}$ values are smaller than those of rigid residues. To identify unusual motion in the SL5 RNA, particularly in its U-turn loop, aromatic ^{13}C (C6/C8) $T_{1\rho}$ relaxation times were determined for all resolved resonances in the ^{1}H−^{13}C correlation spectrum of SL5 (Figure 7). The measured $T_{1\rho}$ values of all C6 and C8 carbons in the SL5 stem, excluding those of

terminal residues, vary from 18.3 to 26.9 ms. The $T_{1\rho}$ values for a particular carbon type (in this case C6 or C8) should be identical for all nucleotides that are rigid with respect to the molecular frame. For SL5, we observed no difference within experimental error between the $T_{1\rho}$ values of C6 and C8 residues, indicating the presence of some internal motions within the helical stem region. These ^{13}C relaxation data indicate that the stem of SL5 does not form a fully rigid structure but may be best described by a semirigid body, given the range of C6/C8 $T_{1\rho}$ values and the high quality of the NMR data for the stem residues. The molecular details of the dynamics in the stem are unclear but may be related to base-pair opening/closing within this small RNA with a marginally stable secondary structure (see Conformation of SL5 section).

The C6/C8 $T_{1\rho}$ values of most loop residues (U696, G697, U700, and A701) fall within the range observed for the stem, indicating that no unusual dynamics characterize these residues. Indeed, the uniformity of the observed C6/C8 $T_{1\rho}$ relaxation times throughout the stem and part of the loop is consistent with a well-ordered RNA structure where the internal motions of most residues are essentially similar. Although U700 is not as well ordered as other bases in the loop (Figure 5a), no unusual dynamics are observed for this base. For U700, the slightly lower precision in the relative position of its base may simply result from the fact that only a few NMR-derived restraints are expected for this extruded base. Interestingly, a significant difference is observed between the C6/C8 $T_{1\rho}$ values of residues A698 (32.5 ± 0.5 ms) and C699 (35.1 ± 1.2 ms) in the loop and those of the stem residues (Figure 7). These larger C6/C8 $T_{1\rho}$ values indicate that these bases are undergoing internal motion on the picosecond to nanosecond time scale. It is important to note that A698 and C699 are involved in two of the three base pairs that stabilize the loop/loop interaction with stem−loop I (*8*) and that their unusual dynamics may be important for this tertiary interaction. More extensive relaxation studies measuring $T_{1\rho}$ as a function of temperature and spin-lock field (*64*) would be necessary to further characterize the motion of the A698 and C699 bases.

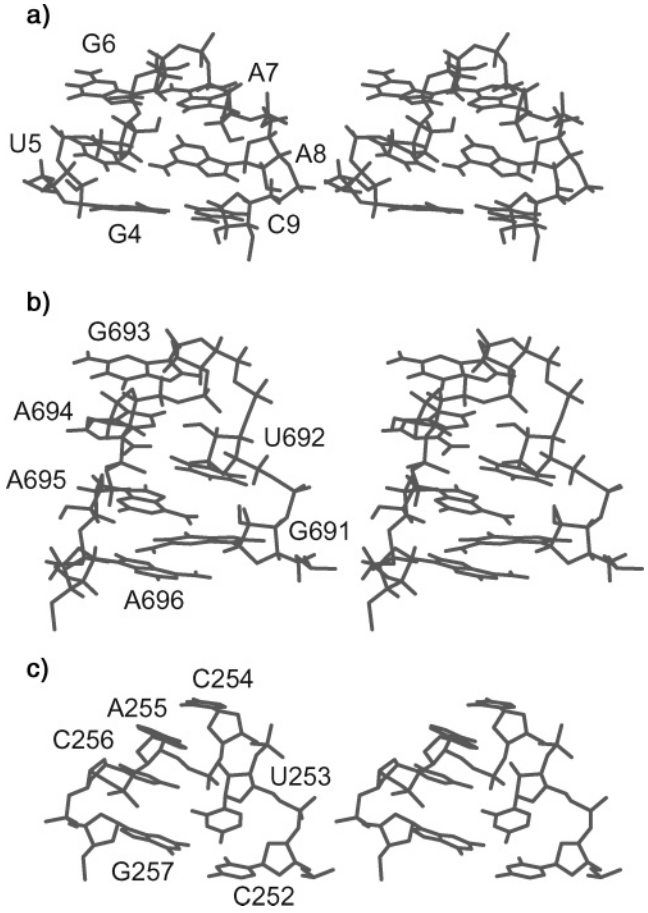

FIGURE 8: Other RNA loop structures with a UNA sequence. (a) Representative NMR structure of the UGAA tetraloop from the eukaryotic 16S-like rRNA [PDB entry 1AFX (*65*)]. This loop does not form a U-turn motif. (b) Representative NMR structure of the 690 loop from the *E. coli* 16S rRNA [PDB entry 1FHK (*66*)]. This RNA loop forms a canonical U-turn structure with residues U692, G693, and A694 representing the UNR sequence. (c) Terminal loop of helix 15 from the 2.4 Å X-ray structure of the large ribosomal subunit of *H. marismortui*. This RNA loop forms a U-turn motif with residues U253, C254, and A255 representing the UNR sequence. As for SL5 RNA, this U-turn is closed by a Watson−Crick base pair (C252-G257) and does not share all the structural charateristics of canonical U-turn structures.

DISCUSSION

Stem−loop V performs at least two important functions in the cleavage mechanism of the VS ribozyme. It participates in the recognition of stem−loop I substrate via a tertiary loop/loop interaction and activates this substrate for catalysis. The stem−loop I/stem−loop V interaction involves the formation of Watson−Crick base pairs between the stem−loop I residues G630−C632 and the stem−loop V residues G697−C699. Formation of this loop/loop interaction is essential for optimal catalytic activity of the VS ribozyme. Our laboratory has initiated structural studies to better understand this RNA/RNA interaction, the effect of divalent metal ions, and the conformational changes involved in formation of this interaction. Here we described the structure of SL5 and we began to investigate the effect of magnesium ions on this RNA. We demonstrated that the loop of stem−loop V forms a U-turn motif in the absence of divalent metal ions, as previously proposed (*8*). Comparison of our SL5 structure with canonical U-turn structures revealed that the SL5 loop lacks three of the seven structural characteristics commonly found in canonical U-turns. Whereas canonical U-turn loop structures are closed by a noncanonical base pair, the loop of SL5 is closed by a Watson−Crick U-A base pair. In addition, the characteristic stacking of the U base and R 5′-phosphate group and hydrogen bond between U H3 and R 3′-phosphate group are not found in the U-turn of SL5. We concluded that SL5 forms a loose U-turn structure in comparison with the more compact backbone fold of canonical U-turn structures.

The less compact U-turn fold of SL5 could be due to a number of factors, including (1) the intrinsic nature of the SL5 loop sequence and (2) the buffer conditions under which the structure was determined. As will be discussed below, increased ionic stength or addition of divalent metal ions could help stabilize a more compact U-turn fold. However, canonical U-turn structures can form in the absence of divalent metal ions and at relatively low ionic strength (*17*). It is important to point out that the UNR sequence may be necessary but is not sufficient for formation of the U-turn motif. This point is illustrated by comparing two RNA tetraloops with the same UGAA sequence (Figure 8a,b). In

the NMR structure of the eukaryotic 16S-like rRNA (*65*), a UGAA tetraloop is flanked by a Watson−Crick G-C base pair (Figure 8a) and does not form a U-turn motif. Instead, in this $U_5G_6A_7A_8$ tetraloop, U5 and G6 are stacked on each other and on the 5′-strand, there is a turn in the backbone after G_6, and the two following As (A7 and A8) are stacked on each other and on the 3′-strand (Figure 8a). In addition, U_5 and A_8 form a noncanonical ribose−base interaction (*65*). Conversely, in the NMR structure of the 690 loop from *Escherichia coli* 16S rRNA (*66*), a UGAA tetraloop forms a canonical U-turn structure (Figure 8b). In this $G_{691}U_{692}G_{693}$-$A_{694}A_{695}A_{696}$ loop, residues U692, G693, and A694 represent the UNR sequence, with the sharp turn in the backbone after U692 and stacking of residues G693, A694, and A695 after the turn (Table 3 and Figure 8b). The loop is closed by a noncanonical sheared G-A base pair between nucleotides G691 and A696. These two examples demonstrate that the UNR sequence UGA, as found in the SL5 loop, is compatible with but not necessarily sufficient for formation of a canonical U-turn structure. How can we explain that this 690 loop forms a U-turn motif and that the 16S-like rRNA UGAA tetraloop does not? Of course formation of a loop with reversal of strand orientation represents a topological problem by itself, which results in added constraints to the phosphodiester backbone. The size of the loop, stacking interactions within and outside the loop, the geometry of the closing base pair, and the presence of modified residues or metal ions can all play a role in defining the most stable loop fold (*65*, *67*, *68*). In the cases of the 690 loop and the 16S-like UGAA tetraloop, the loop sequences are the same, therefore the sizes of the loop are the same, and ionic conditions for structure determination are also comparable. This UGAA tetraloop does not form a U-turn motif, most likely because the backbone is restricted by the Watson−Crick closing base pair and the adjacent helix, as well as by stacking interactions dictated by the closing base pair (*65*). We therefore propose that, in stem−loop V, the UGACU pentaloop structure allows for formation of a U-turn motif but the backbone of this loop closed by a Watson−Crick base pair is too constrained to allow formation of a more compact backbone fold under the conditions used for structural determination (Figure 5).

The closing Watson−Crick base pairs found in the UGAA loop of 16S-like rRNA and in the VS ribozyme stem−loop V may hinder formation of a canonical U-turn structure, and this may explain why in general U-turn loop motifs are closed by noncanonical base pairs (*19*). We have found only two examples in which a consensus UNR sequence forms a U-turn motif closed by a Watson−Crick base pair. In the 30S ribosomal subunit from *Thermus thermophilus*, the UAAC RNA loop of helix H26a is closed by a C-G Watson−Crick base pair and forms a U-turn motif (not shown) (*69*). In the 50S subunit from *Haloarcula marismortui*, the UCAC RNA loop of helix H25 is also closed by a C-G Watson−Crick base pair and forms a U-turn motif (Figure 8c) (*70*). In this $C_{252}U_{253}C_{254}A_{255}C_{256}G_{257}$ loop, the UNR sequence corresponds to residues U253, C254, and A255, with the sharp turn in the backbone after U253 and stacking of residues C254, A255, and C256 after the turn (Figure 8c). Similarly to the SL5 loop, the UAAC loop of 30S helix H26a and the UCAC loop of 50S helix H25 form U-turn motifs but fail to meet all the characteristics of canonical U-turn structures (Table 3). The only missing structural characteristics in these two later cases is the absence of the noncanonical closing base pair and of a hydrogen-bonding interaction between U H3 and R 3′-phosphate group. The U253 N3−A255 3′-P distance in the UCAC loop of 50S helix H25 is 6.79 Å, and the corresponding distance in the UAAC loop of 30S helix H26a is 6.59 Å, more than 2 Å longer than what we measured for canonical U-turn structures (Table 3). Furthermore, in both cases, the relative orientation of the hydrogen-bond donor and acceptor is not compatible with hydrogen-bond formation (Figure 8c). For the SL5 loop, the U696 N3−A698 3′-P distance and their relative orientation are also incompatible with hydrogen-bond formation (Figure 5 and Table 3). The missing hydrogen bond in these structures has previously been recognized as the crucial interaction stabilizing the backbone reversal, because it had been found in all known U-turn structures and is analogous to a G H1−phosphate hydrogen bond in GNRA tetraloops (*19*). However, we find here that this hydrogen bond is not present in U-turns with Watson−Crick closing base pairs. It is interesting to note that, in Watson−Crick base pairs, the C1′−C1′ distance of the paired residues (10.4 Å for A-U base pairs and 10.7 Å for G-C base pairs) (*71*) is larger than that of many noncanonical base pairs, such as sheared G-A base pairs (8.47 Å for the sheared G691-A696 in Figure 8b). This shorter C1′−C1′ distance of the closing base pair may better accommodate the backbone constraints of the U-turn motif. Conversely, the larger C1′−C1′ distance of Watson−Crick base pairs may be incompatible with formation of the hydrogen bond between the U H3 and R 3′-phosphate group, particularly for tetraloops when this hydrogen bond involves loop residues directly adjacent to the Watson−Crick closing base pair. A thorough analysis of all U-turn structures in the database would be necessary to further support our hypothesis that U-turns closed by Watson−Crick base pairs generally lack some important characteristics of canonical U-turn structures.

One important function of U-turns is to facilitate long-range tertiary interactions by exposing to the solvent the Watson−Crick faces of the bases located 3′ after the turn. In stem−loop V, the three bases after the turn (G697, A698, and C699) are stacked on each other and have their Watson−Crick faces exposed to the solvent. Mutagenesis data suggest formation of a three-base-pair antiparallel helical structure between residues G630−C632 of stem−loop I and residues G697−C699 of stem−loop V (*8*). Although the exact conformation of this short helix remains to be determined, it likely resembles that of an A-form helix. To further explore the compatibility of the SL5 structure for formation of the loop I/loop V interaction (*8*), we superposed the heavy atoms of nucleotides G697−C699 with those of an equivalent trinucleotide forming an ideal A-form helix (Figure 9). The RMSD is 1.7 Å for this superposition (Figure 9). Interestingly, nucleotides G697−C699 adopt a conformation that is similar to an A-form helix and compatible with base-pairing formation (Figure 9). Indeed, this superposition indicates that only small displacements of the A698 and C699 bases would be necessary for formation of the modeled interaction (Figure 9). These small base motions could be easily achievable, given the fast internal motion of the A698 and C699 bases (Figure 7) and the availability of space. It is also likely that magnesium-ion binding brings the necessary conformational changes in stem−loop V, since magnesium ions stabilize the tertiary interaction with stem−loop I (*10*).

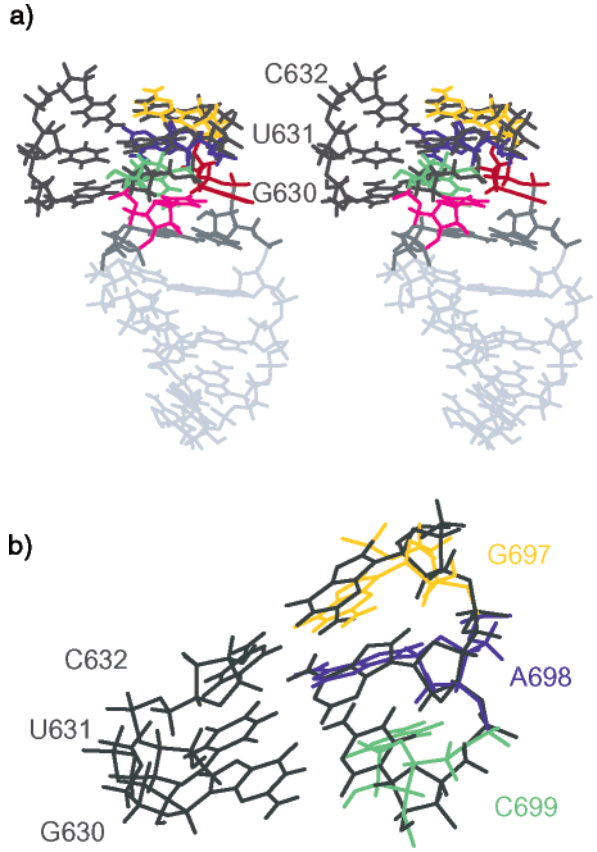

FIGURE 9: Model of the loop/loop interaction between stem−loops I and V. (a) Stereoview of the minimized average structure of SL5 (color-coded as in Figure 1b) superposed on the structure of a three-base-paired A-form helix (in dark gray) formed between a 5′-GAC-3′ and a 5′-CUG-3′ sequence. The superposition was obtained by minimizing the heavy-atom RMSD between the bases of the 5′-GAC-3′ sequences (1.66 Å). (b) Enlarged view of the modeled loop I/loop V interaction from the superposition shown in panel a.

We used chemical-shift mapping to analyze the effect of magnesium ions on the SL5 structure. Changes in chemical shifts were observed for most nuclei and particularly for those in the loop (Figure 6). The lack of confined chemical-shift changes prevented us from localizing magnesium ions onto the NMR structure of SL5. Instead, results from the chemical-shift mapping indicated that multiple magnesium ions are interacting with SL5 or that addition of magnesium ions brings a conformational change in the structure of SL5, or both. The largest changes in chemical shifts were upfield shifts of C699H5 and C699H6 and their attached carbons. These changes in chemical shifts could result from changes in the electronic environment caused by a nearby positively charged magnesium ion (*72*). Indeed, phosphorothioate substitution interference and manganese rescue experiments have indicated that the C699 5′-phosphate group is coordinated to a magnesium ion in the VS ribozyme (*20*). However, the observed changes in chemical shifts (>0.3 ppm) are larger than previously reported for preformed magnesium-ion binding sites in RNA (*72*), indicating that magnesium-ion binding induces a conformational change in the SL5 loop. The large upfield shifts of C699 H5/C5 and H6/C6 could also result from bringing these atoms closer to the center of the ring current of another base. For example, magnesium-ion binding could lead to improved base stacking of C699 with A698 or formation of a stacking interaction between C699 and A701. The large upfield shift also observed for A701 H8 and C8 (Figure 6b) is consistent with magnesium-ion-dependent base-stacking interactions between C699 and A701. These conformational changes could help formation of a more compact SL5 loop structure and stabilization of structural features of canonical U-turn structures not present in the magnesium-ion-free structure of SL5. NMR structure determination of the Mg^{2+}-bound SL5 is currently underway to further understand the effects of magnesium ions on the structure of stem−loop V.

ACKNOWLEDGMENT

We thank B. Golden and J. G. Omichinski for critical reading of the manuscript, J. Brewer for equilibrium ultracentrifugation, J. Boisbouvier and J.-P. Simorre for the CT-TROSY pulse sequence, C. Hoogstraten for the HCCH-E.COSY pulse sequence, and A. Majumdar for the HNN-COSY pulse sequences.

SUPPORTING INFORMATION AVAILABLE

Figure S1, showing the effect of NaCl on SL5 RNA, which includes an overlay of the H6−C6/H8−C8 region of 2D $^{1}H-^{13}C$ CT-HSQC spectra of SL5 at various points of the NaCl titration and comparison of the chemical-shift changes (Δ_T values) after addition of 130 mM $MgCl_2$ and 450 mM NaCl, and Table S1, containing resonance assignments for SL5 RNA. This material is available free of charge via the Internet at http://pubs.acs.org.

REFERENCES

1. Saville, B. J., and Collins, R. A. (1990) A site-specific self-cleavage reaction performed by a novel RNA in *Neurospora* mitochondria, *Cell 61*, 685−696.
2. Kennell, J. C., Saville, B. J., Mohr, S., Kuiper, M. T. R., Sabourin, J. R., Collins, R. A., and Lambowitz, A. M. (1995) The VS catalytic RNA replicates by reverse transcription as a satellite of a retroplasmid, *Genes Dev. 9*, 294−303.
3. Saville, B. L., and Collins, R. A. (1991) RNA-mediated ligation of self-cleavage products of a *Neurospora* mitochondrial plasmid transcript, *Proc. Natl. Acad. Sci. U.S.A. 88*, 8826−8830.
4. Guo, H. C. T., De Abreu, D. M., Tillier, E. R. M., Saville, B. J., Olive, J. E., and Collins, R. A. (1993) Nucleotide sequence requirements for self-cleavage of *Neurospora* VS RNA, *J. Mol. Biol. 232*, 351−361.
5. Andersen, A., and Collins, R. A. (2000) Rearrangement of a stable RNA secondary structure during VS ribozyme catalysis, *Mol. Cell 5*, 469−478.
6. Beattie, T. L., Olive, J. E., and Collins, R. A. (1995) A secondary-structure model for the self-cleaving region of *Neurospora* VS RNA, *Proc. Natl. Acad. Sci. U.S.A. 92*, 4686−4690.
7. Guo, H. C. T., and Collins, R. A. (1995) Efficient trans-cleavage of a stem−loop RNA substrate by a ribozyme derived from *Neurospora* VS RNA, *EMBO J. 14*, 368−376.
8. Rastogi, T., Beattie, T. L., Olive, J. E., and Collins, R. A. (1996) A long-range pseudoknot is required for activity of the *Neurospora* VS ribozyme, *EMBO J. 15*, 2820−2825.
9. Hiley, S. L., and Collins, R. A. (2001) Rapid formation of a solvent-inaccessible core in the *Neurospora* Varkud satellite ribozyme, *EMBO J. 20*, 5461−5469.
10. Andersen, A. A., and Collins, R. A. (2001) Intramolecular secondary structure rearrangement by the kissing interaction of the *Neurospora* VS ribozyme, *Proc. Natl. Acad. Sci. U.S.A. 98*, 7730−7735.
11. Sood, V. D., Yekta, S., and Collins, R. A. (2002) The contribution of 2-hydroxyls to the cleavage activity of the *Neurospora* VS ribozyme, *Nucleic Acids Res. 30*, 1132−1138.
12. Jones, F. D., and Strobel, S. A. (2003) Ionization of a critical adenosine residue in the *Neurospora* Varkud satellite ribozyme active site, *Biochemistry 42*, 4265−4276.

13. Quigley, G. J., and Rich, A. (1976) Structural domains of transfer RNA molecules, *Science 194*, 796−806.
14. Pley, H. W., Flaherty, K. M., and McKay, D. B. (1994) Three-dimensional structure of a hammerhead ribozyme, *Nature 372*, 68−74.
15. Lebars, I., Yoshizawa, S., Stenholm, A. R., Guittet, E., Douthwaite, S., and Fourmy, D. (2003) Structure of 23S rRNA hairpin 35 and its interaction with the tylosin-resistance methyltransferase RlmAII, *EMBO J. 22*, 183−192.
16. Stallings, S. C., and Moore, P. B. (1997) The structure of an essential splicing element: stem loop IIa from yeast U2 snRNA, *Structure 5*, 1173−1185.
17. Puglisi, E. V., and Puglisi, J. D. (1998) HIV-1 A-rich RNA loop mimics the tRNA anticodon structure, *Nat. Struct. Biol. 5*, 1033−1036.
18. Ashraf, S. S., Ansari, G., Guenther, R., Sochacka, E., Malkiewicz, A., and Agris, P. F. (1999) The uridine in "U-turn": contributions to tRNA-ribosomal binding, *RNA 5*, 503−511.
19. Gutell, R. R., Cannone, J. J., Konings, D., and Gautheret, D. (2000) Predicting U-turns in ribosomal RNA with comparative sequence analysis, *J. Mol. Biol. 300*, 791−803.
20. Sood, V. D., Beattie, T. L., and Collins, R. A. (1998) Identification of phosphate groups involved in metal binding and tertiary interactions in the core of the *Neurospora* VS ribozyme, *J. Mol. Biol. 282*, 741−750.
21. Sood, V. D., and Collins, R. A. (2001) Functional equivalence of the uridine turn and the hairpin as building blocks of tertiary structure in the *Neurospora* VS ribozyme, *J. Mol. Biol. 313*, 1013−1019.
22. Cate, J. H., Gooding, A. R., Podell, E., Zhou, K., Golden, B. L., Kundrot, C. E., Cech, T. R., and Doudna, J. A. (1996) Crystal structure of a group I ribozyme domain: principles of RNA packing, *Science 273*, 1678−1685.
23. Milligan, J. F., Groebe, D. R., Witherell, G. W., and Uhlenbeck, O. C. (1987) Oligoribonucleotide synthesis using T7 RNA polymerase and synthetic DNA templates, *Nucleic Acids Res. 15*, 8783−8798.
24. Kao, C., Zheng, M., and Rüdisser, S. (1999) A simple and efficient method to reduce nontemplated nucleotide addition at the 3′ terminus of RNAs transcribed by T7 RNA polymerase, *RNA 5*, 1268−1272.
25. Butler, E. T., and Chamberlin, M. J. (1982) Bacteriophage SP6-specific RNA polymerase. I. Isolation and characterization of the enzyme, *J. Biol. Chem. 257*, 5772−5778.
26. Nikonowicz, E. P., Sirr, A., Legault, P., Jucker, F. M., Baer, L. M., and Pardi, A. (1992) Preparation of ^{13}C and ^{15}N labeled RNAs for heteronuclear multidimensional NMR studies, *Nucleic Acids Res. 20*, 4507−4513.
27. Legault, P., Hoogstraten, C. G., Metlitsky, E., and Pardi, A. (1998) Order, dynamics, and metal-binding in the lead-dependent ribozyme, *J. Mol. Biol. 284*, 325−335.
28. Vuister, G. W., and Bax, A. (1992) Resolution enhancement and spectral editing of uniformly ^{13}C-enriched proteins by homonuclear broadband ^{13}C decoupling, *J. Magn. Reson. 98*, 428−435.
29. Santoro, J., and King, G. C. (1992) A constant-time 2D overbodenhausen experiment for inverse correlation of isotopically enriched species, *J. Magn. Reson. 97*, 202−207.
30. Skleñár, V., Dieckmann, T., Butcher, S. E., and Feigon, J. (1998) Optimization of triple-resonance HCN experiments for application to larger RNA oligonucleotides, *J. Magn. Reson. 130*, 119−124.
31. Pardi, A., and Nikonowicz, E. P. (1992) Simple procedure for resonance assignment of the sugar protons in ^{13}C-labeled RNAs, *J. Am. Chem. Soc. 114*, 9202−9203.
32. Ikura, M., Kay, L. E., Tschudin, R., and Bax, A. (1990) Three-dimensional NOESY−HMQC spectroscopy of a ^{13}C-labeled protein, *J. Magn. Reson. 86*, 204−209.
33. Kay, L. E., Keifer, P., and Saarinen, T. (1992) Pure absorption gradient enhanced heteronuclear single quantum correlation spectroscopy with improved sensitivity, *J. Am. Chem. Soc. 114*, 10663−10665.
34. Simorre, J. P., Zimmermann, G. R., Pardi, A., Farmer, B. T., II, and Mueller, L. (1995) Triple resonance HNCCCH experiments for correlating exchangeable and nonexchangeable cytidine and uridine base protons in RNA, *J. Biomol. NMR 6*, 427−432.
35. Simorre, J. P., Zimmermann, G. R., Mueller, L., and Pardi, A. (1996) Correlation of the guanosine exchangeable and nonexchangeable base protons in ^{13}C/^{15}N-labeled RNA with an HNC-TOCSY-CH experiment, *J. Biomol. NMR 7*, 153−156.
36. Simorre, J. P., Zimmermann, G. R., Mueller, L., and Pardi, A. (1996) Triple-resonance experiments for assignment of adenine base resonances in ^{13}C/^{15}N-labeled RNA, *J. Am. Chem. Soc. 118*, 5316−5317.
37. Mueller, L., Legault, P., and Pardi, A. (1995) Improved RNA structure determination by detection of NOE contacts to exchange-broadened amino groups, *J. Am. Chem. Soc. 117*, 11043−11048.
38. Piotto, M., Saudek, V., and Skleñár, V. (1992) Gradient-tailored excitation for single-quantum NMR spectroscopy of aqueous solutions, *J. Biomol. NMR 2*, 661−665.
39. Grzesiek, S., and Bax, A. (1993) The importance of not saturating water in protein NMR. Application to sensitivity enhancement of NOE measurements, *J. Am. Chem. Soc. 115*, 12593−12594.
40. Legault, P. (1995) Structural studies of ribozymes by heteronuclear NMR spectroscopy, Ph.D. Thesis, University of Colorado at Boulder.
41. Skleñár, V., Miyashiro, H., Zon, G., Miles, H. T., and Bax, A. (1986) Assignment of the ^{31}P and ^{1}H resonances in oligonucleotides by two-dimensional NMR spectroscopy, *FEBS Lett. 208*, 94−98.
42. Dingley, A. J., and Grzesiek, S. (1998) Direct observation of hydrogen bonds in nucleic acid base pairs by internucleotide $^{2}J_{NN}$ couplings, *J. Am. Chem. Soc. 120*, 8293−8297.
43. Hennig, M., and Williamson, J. R. (2000) Detection of NH···N hydrogen bonding in RNA via scalar couplings in the absence of observable imino proton resonances, *Nucleic Acids Res. 28*, 1585−1593.
44. Schwalbe, H., Marino, J. P., King, G. C., Wechselberger, P., Bermel, W., and Griesinger, C. (1994) Determination of a complete set of coupling constants in ^{13}C-labeled oligonucleotides, *J. Biomol. NMR 4*, 631−644.
45. Boisbouvier, J., Brutscher, B., Pardi, A., Marion, D., and Simorre, J. P. (2000) NMR determination of sugar puckers in nucleic acids from CSA-dipolar cross-correlated relaxation, *J. Am. Chem. Soc. 122*, 6779−6780.
46. Delaglio, F., Grzesiek, S., Vuister, G. W., Zhu, G., Pfeifer, J., and Bax, A. (1995) NMRPipe: a multidimensional spectral processing system based on UNIX pipes, *J. Biomol. NMR 6*, 277−293.
47. Johnson, B. A., and Blevins, R. A. (1994) NMRView: a computer program for the visualization and analysis of NMR data, *J. Biomol. NMR 4*, 603−614.
48. Wishart, D. S., Bigam, C. G., Yao, J., Dyson, H. J., Oldfield, E., Markley, J. L., and Sykes, B. D. (1995) ^{1}H, ^{13}C, ^{15}N chemical shift referencing in biomolecular NMR, *J. Biomol. NMR 6*, 135−140.
49. Wijmenga, S. S., Mooren, M. M. W., and Hilbers, C. W. (1993) in *NMR of macromolecules: a practical approach* (Roberts, G. C. K., Ed.) pp 217−288, Oxford University Press, New York.
50. Brünger, A. T. (1992) *X-PLOR 3.1 Manual*, Yale University Press, New Haven, CT.
51. Schwieters, C. D., Kuszewski, J. J., Tjandra, N., and Clore, G. M. (2003) The Xplor-NIH NMR molecular structure determination package, *J. Magn. Reson. 160*, 66−74.
52. Varani, G., Aboul-Ela, F., and Allain, F. H.-T. (1996) NMR investigation of RNA structure, *Prog. NMR Spectrosc. 29*, 51−127.
53. Koradi, R., Billeter, M., and Wüthrich, K. (1996) MOLMOL: a program for display and analysis of macromolecular structures, *J. Mol. Graphics 14*, 51−55.
54. Lavery, R., and Sklenar, H. J. (1988) The definition of generalized helicoidal parameters and of axis curvature for irregular nucleic acids, *J. Biomol. Struct. Dyn. 6*, 63−91.
55. Farmer, B. T. I., Constantine, K. L., Goldfarb, V., Friedrichs, M. S., Wittekind, M., Yanchunas, J. J., Robertson, J. G., and Mueller, L. (1996) Localizing the $NADP^{+}$-binding site on the MurB enzyme by NMR, *Nat. Struct. Biol. 3*, 995−997.
56. Gonzalez, R. L., Jr., and Tinoco, I., Jr. (1999) Solution structure and thermodynamics of a divalent metal ion binding site in an RNA pseudoknot, *J. Mol. Biol. 289*, 1267−1282.
57. Maderia, M., Horton, T. E., and DeRose, V. J. (2000) Metal interactions with a GAAA RNA tetraloop characterized by ^{31}P NMR and phosphorothioate substitution, *Biochemistry 39*, 8193−8200.
58. Yamazaki, T., Muhandiram, R., and Kay, L. E. (1994) NMR experiments for the measurement of carbon relaxation properties in highly enriched, uniformly ^{13}C,^{15}N-labeled proteins: application to ^{13}Cα carbons, *J. Am. Chem. Soc. 116*, 8266−8278.
59. Korzhnev, D. M., Skrynnikov, N. R., Millet, O., Torchia, D. A., and Kay, L. E. (2002) An NMR experiment for the accurate

measurement of heteronuclear spin-lock relaxation rates, *J. Am. Chem. Soc. 124*, 10743−10753.
60. Viles, J. H., Duggan, B. M., Zaborowski, E., Schwarzinger, S., Huntley, J. J. A., Kroon, G. J. A., Dyson, H. J., and Wright, P. E. (2001) Potential bias in NMR relaxation data introduced by peak intensity analysis and curve fitting methods, *J. Biomol. NMR 21*, 1−9.
61. Wijmenga, S. S., and van Buuren, B. N. M. (1998) The use of NMR methods for conformational studies of nucleic acids, *Prog. NMR Spectrosc. 32*, 287−387.
62. Collins, R. A., and Olive, J. E. (1993) Reaction conditions and kinetics of self-cleavage of a ribozyme derived from *Neurospora* VS RNA, *Biochemistry 32*, 2795−2799.
63. Murray, J. B., Seyhan, A. A., Walter, N. G., Burke, J. M., and Scott, W. G. (1998) The hammerhead, hairpin and VS ribozymes are catalytically proficient in monovalent cations alone, *Chem. Biol. 5*, 587−595.
64. Hoogstraten, C. G., Wank, J. R., and Pardi, A. (2000) Active site dynamics in the lead-dependent ribozyme, *Biochemistry 39*, 9951−9958.
65. Butcher, S. E., Dieckmann, T., and Feigon, J. (1997) Solution structure of the conserved 16S-like ribosomal RNA UGAA tetraloop, *J. Mol. Biol. 268*, 348−358.
66. Morosyuk, S. V., Cunningham, P. R., and SantaLucia, J., Jr. (2001) Structure and function of the conserved 690 hairpin in *Escherichia coli* 16S ribosomal RNA. II. NMR solution structure, *J. Mol. Biol. 307*, 197−211.
67. Sundaram, M., Durant, P. C., and Davis, D. R. (2000) Hypermodified nucleosides in the anticodon of $tRNA^{Lys}$ stabilize a canonical U-turn structure, *Biochemistry 39*, 12575−12584.
68. Cabello-Villegas, J., Tworowska, I., and Nikonowocz, E. P. (2004) Metal ion stabilization of the U-turn of the A37 N^6-dimethylallyl-modified anticodon stem−loop of *Escherichia coli* $tRNA^{Phe}$, *Biochemistry 43*, 55−66.
69. Carter, A. P., Clemons, W. M., Jr., Brodersen, D. E., Wimberley, B. T., Morgan-Warren, R., and Ramakrishnan, V. (2000) Functional insights from the structure of the 30S ribosomal subunit and its interactions with antibiotics, *Nature 407*, 340−348.
70. Ban, N., Nissen, P., Hansen, J., Moore, P. B., and Steitz, T. A. (2000) The complete structure of the large ribosomal subunit at 2.4 Å resolution, *Science 289*, 905−920.
71. Saenger, W. (1984) *Principles of Nucleic Acid Structure*, Springer-Verlag, New York.
72. Feigon, J., Butcher, S. E., Finger, L. D., and Hud, N. V. (2001) Solution nuclear magnetic resonance probing of cation binding sites on nucleic acids, *Methods Enzymol. 338*, 400−420.
73. Scott, W. G., Murray, J. B., Arnold, J. R. P., Stoddard, B. L., and Klug, A. (1996) Capturing the structure of a catalytic RNA intermediate: The hammerhead ribozyme, *Science 274*, 2065−2069.
74. Shi, H. J., and Moore, P. B. (2000) The crystal structure of yeast phenylalanine tRNA at 1.93 Å resolution: A classic structure revisited, *RNA 6*, 1091−1105.

BI047963L